Synergistic Factors Affecting Catalytic Performance of Fe(II) Phthalocyanine @ Titania-Pillared Bentonite Nanocomposites in Styrene Production

Salah A. Hassan[1], Fatma Z. Yehia[2], Hamdy A. Hassan[1] and Atef S. Darwish[1,*]

[1]*Department of Chemistry, Faculty of Science, Ain Shams University, Cairo, Egypt*

[2]*Department of Petrochemicals, Egyptian Petroleum Research Institute, Cairo, Egypt*

Abstract: The hybrid nanocatalytic system under study consisted of iron (II) phthalocyanine complex (FePc) of 0.5 – ~10 wt % loading immobilized in the bentonite interlayers modified by pillaring with titania nanoparticles (88 nm). Various interactions facing FePc complex were discussed through the changes in different characteristics assessed by adopting XRD, FTIR, ICP-EDX, TGA-DrTGA, TEM, N_2 adsorption-desorption and H_2-chemisorption techniques. Intercalated FePc molecules could evolve excessive silanol and aluminol sites through interaction with various clay-interlayer sites and titania pillar. By applying this FePc @ Ti-PILB nanocomposite in oxidative dehydrogenation of ethyl benzene, synergistic combination of factors influencing selective production of styrene confirmed the optimum turnover frequency with maximum selectivity to styrene at 3.4 wt % FePc loading. Below this loading, redox pair factor linked with dispersion and orientation mode of FePc was predominating. In higher loaded samples of considerable silanol sites, clay acid-base pair balance became prevailing.

Keywords: Iron (II) Phthalocyanine, Ti-Pillared Bentonite, Oxidative dehydrogenation, Styrene production, Synergistic factors.

1. INTRODUCTION

Bentonite, as smectite type clay mineral, is widely used in different industrial fields due to its swelling, colloidal and rheological properties as well as high cation exchange capacity [1-3]. Such properties encourage bentonite to be capable of intercalating organic and inorganic molecules in its interlayer space. The edge surface of bentonite consists of alumina and silica sites with broken bonds formed during the crystal growth [4]. Dissociable surface sites are formed by breaking the O-Si-O and O-Al-O bonds, where exposed Si sites, modeled as acidic silanols, behave like the pure oxide. Edge Al sites, modeled as amphoteric aluminols, undergo protonation at low pH and deprotonation at high pH [5-7].

In order to remove impurities and various exchangeable cations from smectite to be used as an adsorbent or as a catalyst, different treatments have been applied, most frequently with inorganic acids [8, 9] or through pillaring with polyoxocations [10, 11]. Acid treatment could decrease the spacing between adjacent layers, produce finely dispersed silicon oxide from destruction of mineral structures and form cracks and voids in the surface [3, 8, 9]. Pillared interlayered clays (PILC's) could be prepared by exchanging charge compensating cations in the interlayers with polymeric hydroxyl metal cations to give oxide pillars by calcination, creating interlayer and interpillar spaces[12]. Pillaring with titania provided the clay with higher surface area, adsorption ability, thermal and hydrothermal stability and additional acid sites, as compared with other metal oxide PILC's [13] favoring distinguished efficiency of Ti-PILC in different catalytic processes [14-16]. For example, the enhanced porosity allowed shape selective catalysis on Ti-PILC to form ethyl benzene as the only product in ethylation of benzene [16]. Dispersion of anatase in clay layer structure was controlling factor in the photocatalytic degradations [17].

On the other hand, researches have continued for a long time towards finding new varieties of catalysts and less severity of reaction conditions for the dehydrogenation of ethyl benzene to styrene, an important monomer used in plastic and rubber industries. Among the known dehydrogenation catalysts, promoted and supported Fe_2O_3 have long been used as standard catalysts, especially in the presence of large quantity of steam at high temperatures of 600 – 700^{0}C and in the presence of CO_2, which is one of greenhouse gases causing global warming [18-21]. However, within trials to overcome the process equilibrium limitations and high energy consumption, appeared our guide work on application of nickel phthalocyanine (NiPc) / Indian bentonite as a new selective catalyst for styrene production [22]. The

*Address correspondence to this author at the chemistry department, faculty of science, Ain-Shams University, Cairo 11566, Egypt;
Tel: +202 24831836; Fax: +202 24831836;
E-mail: atef_mouharam@sci.asu.edu.eg

E-ISSN: 2408-9834/15

relatively higher activity of the catalyst sample of 1.0 wt % complex loading was discussed in view of the orientation and facile accessibility profiles of NiPc in clay layer structure to reactant molecules. The immobilized metal phthalocyanine complexes into silicate structures, *e.g.*, bentonite clay, exhibited considerable stability against dimerization, formation of inactive μ-oxo structures and other destructive events, displaying marked reactivity in various oxidation processes [23-27]. The complex centers located in clay galleries did not contribute largely to catalytic activity, whereas the accessibility of complex centers at external edge sites was more important to overall activity of the immobilized catalyst [25, 28, 29]. From literature survey, only limited works have dealt with intercalated complexes into pillared clays interlayers [28, 30, 31]. For example, no sufficient attention has been paid to the application of intercalated iron (II) phthalocyanine (FePc) into titania–pillared bentonite (Ti-PILB) in oxidative dehydrogenation reactions. FePc, being analogous to biomimetic iron porphyrin, can serve as a prosthetic group of hemoglobin (as oxygen carrier) and as a model for catalytic action of Cytochrome P-450 in oxidation processes, which favor its effective use under atmospheric oxidative conditions.

In the present study, the standard supported Fe_2O_3 was replaced by Fe (II) phthalocyanine (FePc) immobilized in different loadings (in the range, 0.5 – ~10 wt %) into Ti-PILB, to be functioned in the production of styrene through oxidative dehydrogenation (ODH) of ethyl benzene (EB) at mild atmospheric conditions. Different changes induced by incorporation of varying extents of the complex into the modified bentonite layer structure were discussed through structural, textural, thermal, acid-base and complex dispersion characteristics of the formed hybrid FePc @ Ti-PILB catalytic system. Various catalytic activity parameters were discussed in view of the synergism involving the reactive interlayer sites, pillar species and intercalated complex molecules hosted between modified clay layers.

2. EXPERIMENTAL

2.1. Preparation of Titania-Pillared Bentonite Clay (Ti-PILB)

For pillaring purposes, pure potassium and calcium-rich bentonite (PROLABO) was first acid activated by using 6M HCl solution (in a solid/liquid molar ratio = 1:15) for 18 h at 70^{o}C. After removing the acid and washing several times with deionized water until pH = 6, the produced paste was dried at 100^{o}C for 18 h and calcined at 300^{o}C for 4 h. The fresh pillaring solution, prepared from $TiCl_4$ (BDH) in 6M HCl, diluted to a H^+/Ti ratio = 1:11, was added drop wise to 500 cm^3 of a suspension containing 30 g of acid/thermally activated bentonite, achieving a final Ti/clay ratio = 0.60 mmol g^{-1} [15, 32]. The finished product was filtered, washed with distilled water and calcined for 4 h at 300^o C in a flow of dry air.

2.2. Preparation of Iron (II) Phthalocyanine @ Ti-PILB Nanocomposite System

Synthesis and modification of iron (II) phthalocyanine (β-FePc) were performed as described else where [33, 34] by adding ferrous salt (8.5 g) in portions to a stirred mixture of phthalimide (50 g), urea (95 g), ammonium chloride (22 g) and ammonium molybdate catalyst (0.68 g) in nitrobenzene (115 ml) at 180^o C. The reaction mixture was refluxed for further 5 h at 180^{o}C and then filtered while hot. The separated complex was washed with hot water and refluxed with methanol. The produced fine crystals were dried at 100^{o}C for 10 h, purity of which was checked through UV-visible analysis, mainly at λ_{max}= 683 nm in $CHCl_3$.

For immobilizing FePc into Ti-PILB, an appropriate quantity of the complex was dissolved in 1.0 M H_2SO_4 under reflux conditions for 1 h [28, 34]. A known amount of the pillared clay was added while reflux was continued for further 10 h. The catalyst sample was filtered, washed with distilled water, dried for 12 h at 100^{o}C and calcined for 4 h at 260^{o}C in airflow. By analysis, FePc loadings were found to be: 0.5, 1.0, 4.78, 7.0 and 9.67 wt %, corresponding to fractional degree of surface coverage (α_{FePc}) = 0.1, 0.2, 0.7, 1.0 and 2.0, respectively [22]. For simplicity, the samples were designated as x FePc @ Ti-PILB, where x denotes FePc loading.

2.3. Characterization Techniques

Structural characteristics of acid-treated (ATB) and titania-pillared bentonite (Ti-PILB) as well as various immobilized FePc @ Ti-PILB samples were investigated through conventional techniques, viz., XRD using a Philips PW3710-BASED diffractometer, operated with Ni-filtered Cu Kα radiation (λ= 1.5418 Å) at 40 kV and 55 mA, and FTIR using ATi Mattson WI 53717 model Genesis spectrometer, USA, with a resolution of 2 cm^{-1}. Chemical analysis was performed through energy dispersive X-ray spectroscopy (EDXS)

on JEOL JSM-840 A, Oxford model 16211, with a resolution of 1.3 eV. Diffraction traces were taken in RIGAKU D/MAX-C instrument using Cu Kα radiation (λ = 1.5405 Å). The metal ratios were also determined using inductively coupled plasma (ICP-OES) on Jobin-Yvon instrument (JY-24), applying microwave digestion in an Anton Paar multi-wave instrument.

Thermal analysis of various samples was performed on a Perkin-Elmer instrument using α-alumina as a reference. Temperature programming rate was 5.0°C min^{-1}, up to 700°C in atmospheric air, adopting CR3A recorder.

The texture of different solid systems was investigated via BET surface area determination and pore analysis, based on N_2 adsorption-desorption isotherms at -196°C [35] using a NOVA 3200 apparatus, USA. Initial pretreatment of samples involved outgassing for 4 h at 200°C. Their morphology was studied through scanning electron microscopy (SEM) on a JEOL JSM-5400 working at 30 kV and transmission electron microscopy (TEM) on a JEOL 1200 EX II at 120 kV with 0.2 nm resolution.

Chemisorption of pure H_2 was applied for estimating the degree and mode of dispersion of the immobilized FePc in studied systems [36]. The chemisorption isotherms were measured at 300° C using a micro volumetric apparatus up to P_{eq}~ 250 Torr (1 Torr = 1.33 x 10^2 Pa). The net adsorption uptakes, n_{H2}, (in mmol H_2 g^{-1} sample) were determined from the isotherms, after correction for the neat Ti-PILB support. The apparent degree of complex dispersion $[D_{FePc}]_{app}$ was calculated as the ratio of n_{H2} (or equivalently number of surface FePc molecules [n_{FePc}]) : total number of FePc molecules in the sample. Surface area of immobilized complex (S_{FePc},$m^2g^{-1}{}_{FePc}$) and stoichiometry of H_2 adsorption ($n_{H2}/n_{Fe}{}^{2+}$) were also calculated, to assess the orientation models [22, 24, 36].

The cation exchange capacity (CEC) was estimated, in mequiv./100g, by the aid of copper bis-ethylenediamine complex $[Cu\ (en)_2]^{2+}$ method [37]. Changes in the surface acid–base behavior were followed up potentiometrically [38] adopting a suggested three-site model [39, 40]. Based on this model,various surface charge site densities could be derived from the potentiometric titration curves, according to pH ranges of the measurements. The site density of amphoteric aluminols (D_{AlOH}) was derived from the number of edge aluminol surface charges, $\sigma_{H\ (edge)}$, (at pH range 5 – 8). The basal plane cation exchange site density (D_{CE}) was based on the number of basal proton surface charges, $\sigma_{H\ (basal)}$, estimated from CEC [39, 41] (at pH ≈ 4). The site density of acidic silanols (D_{SiO^-}) was calculated from the number of edge silanol surface charges, $\sigma_{O^-(edge)}$ (at pH> 8). The surface charge site densities, D_x (sites nm^{-2}), could thus be determined according to the equation [40, 42]:

$$D_x = \sigma_x\ (\text{mmol } L^{-1}\ g^{-1}) \times N_{Av} / S_{BET}$$

where, N_{Av} is Avogadro's number and S_{BET} ($nm^2\ g^{-1}$) is the specific surface area of the sample. Point of zero net proton charge (PZNPC) was also estimated [40].

2.4. Activity Measurements

The oxidative dehydrogenation (ODH) of ethyl benzene (EB) was performed in a tubular fixed bed reactor (190 mm x 35 mm i.d.), under atmospheric conditions [43]. A catalyst sample of 0.5 g, mixed with glass beads, was pre-activated at 250° C for 2h. EB was introduced into the reactor by means of a micro-dose pump, Unipan type 335 A, in a feed rate (F) = 2 ml h^{-1}, together with the dynamic air controlled by a flow controller, Brooks 5850^E. The condensed product samples were analyzed byGLC using a stainless steel column (10 ft x 3 mm e.d.) packed with 5% bentonite 34 and 5% diisodecyl phthalate on Chromosorb PAW (80-100 μm mesh size). The column temperature was programmed in the range 80°C – 200°C (in the rate of 20°C min^{-1}) and the FID temperature was fixed at 200°C. Styrene (Sty) was the main reaction product, with smaller amounts of benzene (B) and toluene (T). The degree of EB conversion (X, %) and fractional selectivity to styrene (S_{Sty}, %) could be calculated as:

$$X = [1 - (g_{EB\ out}/g_{EB\ in})] \times 100, \text{ and}$$

$$S_{Sty} = [(F_{Sty}/ \sum (F_{Sty} + F_B + F_T)] \times 100$$

where, g_{EBout} is the mass of exhausted EB for a given period, $g_{EB\ in}$ is the mass of EB introduced to the system for the same period and F_{Sty}, F_B and F_T are the molar fractions of Sty, B and T, respectively, in the final products, estimated from the corresponding chromatographic peak areas.

3. RESULTS AND DISCUSSION

3.1. Structural Characteristics of Various FePc @ Ti-PILB nanocomposite Samples

3.1.1. XRD Analysis

The XRD patterns in the low angle range of acid treated bentonite (ATB), titania–pillared bentonite (Ti-

PILB) and various FePc @ Ti-PILB samples are shown in Figure **1**. Basal (001) d-spacing, full width at half maximum peak height (FWHM) of basal d(001) and relative intensities of most characteristic peaks are given in Table **1**. For both modified bentonite supports, basal (001) reflection at 2Θ ≈ 5.75°, corresponding to d-spacings of 15.22 and 15.28 Å, can be linked with the presence of Ca- and Na- montmorillonite as dominant clay mineral in pure bentonite [37]. Compared with pure bentonite, the marked decrease in intensity of basal diffraction peak (I_{001}), particularly in Ti-PILB, and the pronounced increase in intensity of (101) peak at 2Θ = 21.8° (I_{101}) of OCT (opal para-crystalline silica) reflect the acid attack of octahedral layer, exposing the tetrahedral layer [44]. The considerable increase in basal $FWHM_{001}$ value and in intensity of (02) and (11) peak, of two-dimensional (hk) reflections, confirms the enhanced deformation of layer stacking with dealumination and/or delamination of the clay galleries [45]. The existence of nano-sized titania pillar in clay interlayers may be evidenced from the weak peak appeared at 2Θ = 25.7°, characteristic of anatase,the average particle size of which is ~88 nm as estimated by Scherer equation adopting the corresponding FWHM value [28, 45].

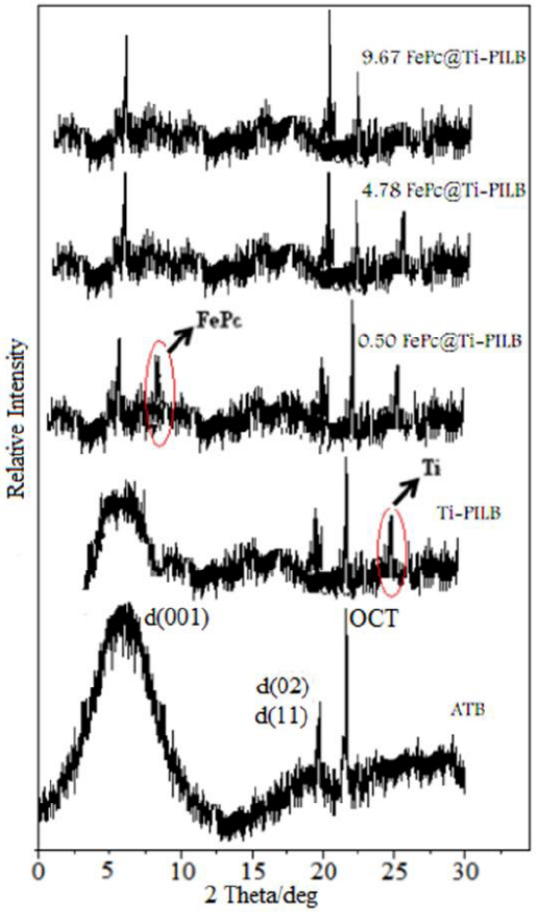

Figure 1: XRD patterns of: ATB and Ti-PILB supports and immobilized FePc @ Ti-PILB nanocomposites of different complex loadings (wt %): (1) 0.50, (2) 4.78 and (3) 9.67.

From XRD patterns of the immobilized FePc samples of different loadings, the incorporated complex seems to bind the clay layers, as ensured by the reduction in d_{001} basal spacing and marked decrease in $FWHM_{001}$ (Table **1**). As d_{001} shows a gradual increase with increasing the complex loading, up to 9.67 wt %, a continual intercalation of FePc molecules into clay galleries can be suggested, accompanied probably with a change in complex orientation and more attack of tetrahedral silica bridges (cf., more intense (02) and (11) peak, sharp decrease in I_{101} and a broader peak of OCT, Figure **1**). For diluted 0.5 FePc@Ti-PILB sample, a characteristic peak of FePc could be detected, referring to collection of the complex molecules at layer edges restricted mostly by the located titania pillar in the interlayers. For the increased complex loadings, disappearance of the characteristic peak of FePc, associated with a diminution in the anatase peak intensity, can point to probable interactions of FePc molecules with both nanotitania pillar and various interlayer sites.

3.1.2. FTIR Analysis

FTIR spectra of modified bentonite supports (ATB and Ti-PILB) and of a representative immobilized 4.78 FePc @ Ti-PILB sample are depicted in Figure **2**. For ATB, deformation of the original bentonite octahedral sheet structure by acid treatment is confirmed by appearance of a significant band of coupled Al–O and Si–O out-of-plane vibrations at 620 cm^{-1} and of para-crystalline silica (OCT) at 784 cm^{-1}, with elimination of AlAl–OH, AlFe–OH and AlMg–OH bending bands around 908 cm^{-1} and of Al–O–Si bending band at 514 cm^{-1} [28, 44]. The whole layer structure of parent bentonite is remained almost intact by such treatment, preserving same intensities of Si–O–Si in-plane stretching bands in the 1000–1200 cm^{-1} region and of Si–O–Si bending band at 467 cm^{-1}[44]. For Ti-PILB, weakened band at 780 cm^{-1} of amorphous silica and the new one appeared at 979 cm^{-1} of Ti–O–Ti confirm the location of Ti polyoxocations in clay interlayers, probably in weaker electrostatic interaction with silica tetrahedral sheets. Ti–O–Si and Ti=O bands of strong covalent interactions are absent [46].

For the immobilized FePc sample, overlapping of the strong Si-O-Si vibrations [44] in 940–1260 cm^{-1}

Table 1: XRD Parameters of Most Characteristic Peaks for Parent and Modified Bentonite Supports and Different FePc @ Ti-PILB Nanocomposite Systems

Samples	d_{001} I_{001} $FWHM_{001}$			$I_{02\ \&\ 11}$	I_{101}
	(Å)	(%)	(°)	(%)	(%)
Pure bentonite	15.34	100	0.06	19	31
ATB	15.22	60	0.40	53	100
Ti- PILB	15.28	16	0.32	55	100
FePc@Ti-PILB of FePc wt %:					
0.50	13.48	37	0.06	57	94
4.78	13.58	34	0.08	64	30
7.00	13.83	34	0.10	100	11
9.67	14.38	55	0.08	100	29

region with most characteristic bands of FePc and disappearance of both 620 cm^{-1} and 979 cm^{-1} bands may confirm the interaction of the complex with Ti-pillar located in the clay interlayers, probably at exposed Si-tetrahedral sites.

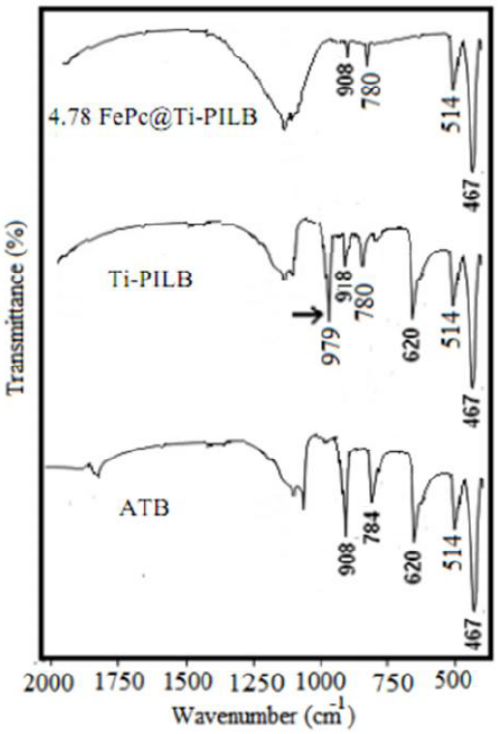

Figure 2: FTIR spectra of: ATB, Ti-PILB and 4.78 FePc @ Ti-PILB nanocomposite.

3.1.3. Thermo-Gravimetric Analysis (TGA)

The differential thermo-gravimetric profiles (DrTGA) of modified ATB and Ti-PILB supports and the representative 4.78 FePc @ Ti-PILB sample are presented in Figure **3**. For the acid treated bentonite (ATB), some weight loss in a single step is observed between ~50 and 180°C, corresponding to evolution of physisorbed and interlayer water from silicate sheets, as revealed in the original bentonite. Marked thermal stability is then noticed up to> 650°C, in contrast to the untreated bentonite, where steps at 380°C – > 550°C, of loss of lattice OH's [22] disappear. For Ti-PILB, DrTGA profiles indicate relatively easier dehydration in first step. Introduction of titania nanoparticles in clay interlayers seems to expose several interactive OH sites, interaction products of which exhibit dehydroxylation in steps [13]. Smaller steps maximized at ~ 230°C and ~ 340°C may be linked with dehydroxylation of weakly interacted tetrahedral silanols and titanium pillaring moieties [13] respectively. Due to stronger interaction of Ti-pillar with clay edge OH's, decomposition of the product appears at ≥ 480°C [47].

For the immobilized 4.78 FePc@Ti-PILB sample, DrTGA profiles confirm deeper intercalation of FePc molecules in the modified clay galleries, probably interacted with interlayer and exchange sites, showing thereby several dehydroxylation / decomposition steps. The steps at ~50°C and 100 °C correspond to gradual

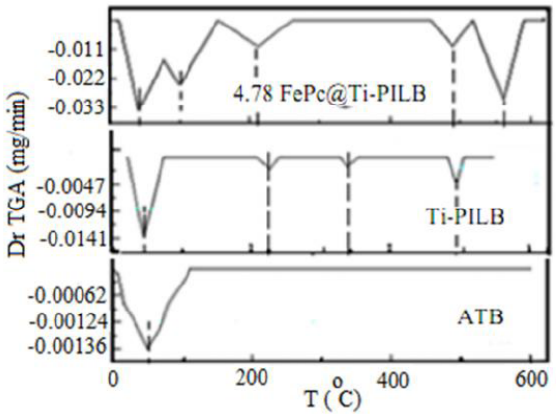

Figure 3: Differential thermo-gravimetric profiles of: ATB, Ti-PILB and 4.78 FePc @ Ti-PILB nanocomposite.

loss of physisorbed and interlayer water from silicate sheets, respectively. Dehydroxylation step of silanols at 220^{o}C is larger than that in neat pillared clay due to complex attack of tetrahedral silica bridges. Decomposition of stronger interaction product involving Ti pillar, FePc and edge OH's is occurred at ~ 480 ^{o}C (pure FePc starts to decompose in the region, 360 – 440^{o}C [22]), followed by collapse of pillared clay structure at ≥ 560^{o}C [22, 47].

3.1.4. Elemental Analyses, Cation Exchange Capacities and Surface Charge Site Densities

As reported previously, dissociable sites on edge surfaces of phyllosilicate are formed through different attacks by breaking of O-Si-O and O-Al-O bonds, exposing thereby several interactive silanol and aluminol sites [4-6]. Exposed silanols (SiO^{-}) are related to BrÖnsted acidity in the inter-lamellar region and exposed aluminols (AlOH) are linked with Lewis acidity mainly at edges, while cation exchange capacity (CEC) is associated with Lewis acidity arising from structural defects, broken bonds and hydroxyl transfers [3, 28, 39].

Elemental analysis data, by EDX and ICP, of modified bentonite supports (ATB and Ti-PILB) and different immobilized FePc @ Ti-PILB samples are summarized in Table **2**. For acid activated bentonite (ATB), the increase in Si/Al ratio can be attributed to dealumination of the octahedral sheet, where most of exchangeable cations in interlayers are leached out, especially Ca^{2+} and Mg^{2+}. This may be evidenced by some decrease in CEC and Si and Al percentages of the pure bentonite. Lowering in PZNPC refers to proton trapping during the activation process. For Ti-PILB, deeply intercalated titania nanoparticles into modified interlayers seem to face some interactions, mainly with tetrahedral silica, through occupation of some exchange sites (cf., further decrease in CEC). Lower PZNPC value can be linked with protons intercalation associated with titania pillaring.

By immobilizing FePc (from 0.5 to 9.67 wt %) into Ti-PILB support, a gradual decrease in total content of exchangeable cations (cf., M, and CEC, Table **2**) may point to excessive interactions of the complex with various interactive/exchange sites in clay interlayers. Extent of attack of silica bridges obviously exceeds that one of alumina bridges. This can be linked with marked increases in surface charge site densities, $D_{SiO^{-}}$,D_{AlOH}, and D_{CE}, of BrÖnstedsilanol, Lewis aluminol and cation

Table 2: Main Data Derived from EDX and ICP Analyses, Aggregation Factors (X_{Ti} and X_{FePc}), Cation Exchange Capacities (CEC) and Point of Zero Net proçton Charge (PZNPC) for Neat bçentonite supçports and Different FePc@Ti-PILBnanocomposites

Samples	Composition by EDX (%)					M	Si/Al	X_{Ti}	X_{FePc}	CEC (meq/100g)
	Si	Al	Mg	Ca	K	(μmol /g)				(PZNPC)
Pure bentonite	34.98	4.47	0.44	1.46	1.83	589	6.7	-----	-----	66.9 (10.14)
ATB	33.67	3.35	0.00	0.00	1.49	380	9.2	-----	-----	62.0 (8.64)
Ti- PILB	23.45	3.07	0.25	0.00	0.98	466	6.7	2.00	-----	55.0 (8.88)
FePc@Ti- PILB of FePc wt %:										
0.50	22.18	2.84	0.12	0.00	0.90	406	7.2	1.83	1.40	92.7 (4.15)
1.00	17.70	2.66	0.00	0.00	0.82	377	7.0	1.78	1.15	38.2 (4.36)
4.78	14.13	1.82	0.00	0.00	0.52	342	7.1	0.87	2.40	39.6 (4.19)
7.00	15.00	2.10	0.00	0.00	0.50	335	6.8	1.12	1.80	39.6 (4.19)
9.67	14.13	1.87	0.16	0.00	0.52	325	7.0	1.00	2.20	50.3 (4.83)

exchange sites, respectively, by increasing the complex loading, particularly > 1.0 wt % (Figure **4**), and with significant lowering of PZNPC toward more acidic behavior. By some interaction of FePc with titania pillar, new exchange sites seem to be regenerated.

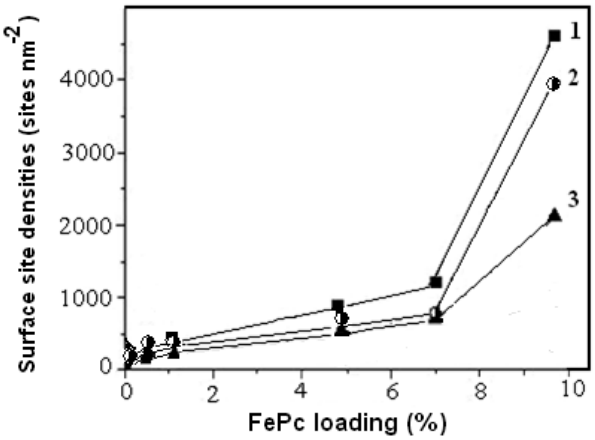

Figure 4: Surface charge site densities of: 1. Silanols (D_{SiO^-}), 2. Aluminols (D_{AlOH}), and 3. Cation exchange(D_{CE}) as a function of FePc loading in FePc@Ti-PILB nanocomposite systems.

To confirm interactions facing the incorporated titania pillar and intercalated FePc complex into modified bentonite clay layers, an aggregation factor (X) was suggested [28] (Table **2**). This factor was taken as the ratio of theoretically calculated concentration used in preparing the concerned "monomeric" species / experimentally found concentration from ICP analysis. Aggregation factor of titania (X_{Ti}) found to be ~2 in neat Ti-PILB support and in diluted FePc @ Ti-PILB samples (of 0.5 and 1.0 wt % FePc) indicates the accumulation of Ti-pillar in flocculated particles at clay edges. In higher loaded samples (of 4.78 and 9.67 wt % FePc), X_{Ti} = ~1, pointing to probable dissociation of aggregated titania species through stronger interaction with interlayer sites and/or FePc molecules. FePc complex in diluted samples (of 0.5 and 1.0 wt % FePc) seems to exist as monomeric disk shaped molecules (X_{FePc}= ~1), oriented at layer edges. In higher loaded samples (of 4.78 and 9.67 wt % FePc), the complex most probably exists as dimeric aggregates (X_{FePc} = ~2).

3.2. Textural and Morphological Characteristics of the Investigated Samples

The adsorption-desorption isotherms of N_2 at -196° C for the neat Ti-PILB support and various samples of immobilized FePc @ Ti-PILB system are of type II in IUPAC classification (Figure **5**, A) [35]. For the neat support and diluted immobilized samples (of 0.5 and 1.0 wt % FePc), the closed hysteresis loops are of type H3, characteristic of slit-shaped pores. For higher loaded samples, the isotherms tend almost to be reversible, referring to evolution of larger fraction of mesoporosity. Table **3** summarizes surface parameters derived from the isotherms, viz., specific surface areas ($S_{BET,}$ m^2 g^{-1}), pore volumes ($V_{p,}$ ml g^{-1}) estimated at 0.95 p/p_o and average pore radii ($\bar{r}_p^{pp}$) assuming parallel plate (pp) pore model. A significant increase in surface area and total pore volume by acid treatment (ATB) and by titania pillaring (Ti-PILB) of pure bentonite may be related to deformation of octahedral sheet structure, permitting incorporation of Ti nanoparticles in the clay interlayers. The common decrease in surface area of immobilized FePc samples, together with a marked increase in pore mouth dimensions ($\bar{r}_p^{pp}$), can be attributed to accumulation of a fraction of the complex at layer edges, during its intercalation into Ti-PILB pore system.

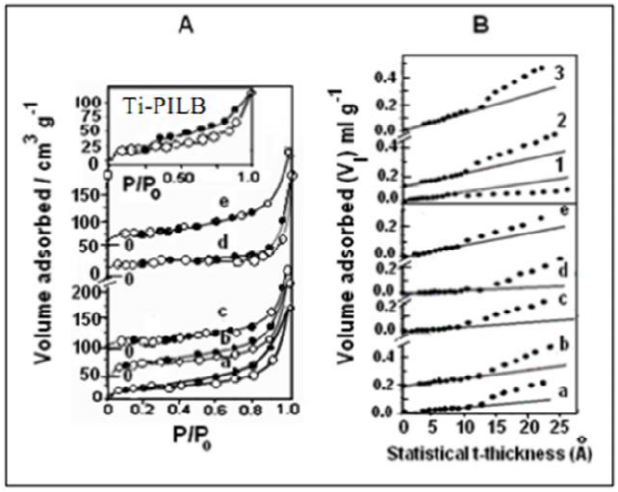

Figure 5: A: N_2 adsorption-desorption isotherms at -196 °C on neat Ti-PILB (inset) and various FePc@Ti-PILB nanocomposites of different FePc loadings (wt %): a- 0.50, b- 1.00, c- 4.78, d- 7.00 and e- 9.67. B: V_l-t plots for: 1- pure bentonite, 2- ATB, 3- Ti-PILB and various FePc@Ti-PILB nanocomposites of different FePc loadings (wt %): a- 0.50, b- 1.00, c- 4.78, d- 7.00 and e- 9.67.

For assessment of pore characteristics, V_l-t plots are constructed based on obtained isotherms, where (V_l) is the volume of N_2 adsorbed in ml g^{-1} and (t) is the statistical thickness in Å [22, 36]. Reasonable agreement between S_{BET} and S_t (calculated from slopes of V_l – t plots) is the main criterion for correct choice of the t–curve used (Table **3**). The V_l– t plots for various samples under study, using roughly the reference t-curve of Sing *et al*. [35] are depicted in Figure **5**, B. The plot for pure bentonite shows a downward deviation

Table 3: Surface Parameters of Neat Bentonite Supports and Different Immobilized FePc@Ti-PILB Samples

Samples	S_{BET} ($m^2 g^{-1}$)	$V_{p,}$ ($ml\ g^{-1}$)	r_p^{pp} (nm)	S_t ($m^2 g^{-1}$)	$r_h^{pp}{}_{most\ abund}$ (nm)
Pure bentonite	20.38	0.0480	4.73	25.67	0.92 - 1.16
ATB	65.68	0.1866	5.68	58.29	0.92 - 1.86
Ti- PILB	78.41	0.1871	4.77	74.44	1.83
FePc@Ti-PILB of FePc wt %:					
0.50	40.23	0.1667	8.29	39.26	1.88 - 3.80
1.00	65.23	0.2031	6.23	60.65	1.84
4.78	23.50	0.1182	10.06	26.54	1.33- 1.62
7.00	13.09	0.1372	20.96	14.19	1.55
9.67	47.56	0.1606	6.75	46.00	1.27- 1.46

starting at t–values ~ 9 – 10 Å, linked with a predominating fraction of micropores. However, for modified ATB and Ti-PILB supports as well as various immobilized FePc samples, upward deviation in the V_l–t plots show increasing slopes, indicating existence of wider groups of mesopores. These findings can be confirmed by the most abundant pore radii ($r_h^{pp}{}_{mostabund}$) derived from pore size distribution (PSD) curves [22] applying the parallel plate pore model (Table **3**). The original bentonite shows a smaller fraction of micropores of most frequent hydraulic radius of ~9 Å, representing the thickness of TOT layer, beside larger fraction of pores of ~12 Å. While in ATB, acid treatment leads to an increase in radius of larger fraction of pores to 18.6 Å, incorporation of aggregated pillar into the acid treated clay interlayers tends to eliminate a number of micro-sized pores. For diluted FePc@Ti-PILB samples (< 1.0 wt % FePc), creation of additional fraction of mesopores of wider mouth dimensions (38 Å) may be related to accumulation of most of oriented complex molecules at layer edges. By increasing FePc loading > 1.0 wt %, some decrease in most frequent pore radius (to 12-15 Å) can be referred to the crowded complex molecular clusters in the interlayers, without affecting the overall tactoidal structure.

For more confirmation, TEM micrographs for selected samples of FePc @ Ti-PILB system are compared with those of pure bentonite and neat Ti-PILB support in Figure **6**. The crystalline-layered structure of the parent bentonite is clear in micrograph (a). As seen in micrograph (b) for Ti-PILB, titania pillar nanoparticles, of an average size around 84 nm (compared with 88 nm from XRD data) are incorporated into the deformed clay structure. In micrograph (c) for a diluted catalyst sample (of 0.5 wt % FePc), finer complex aggregates of 2 – 4 nm sizes are shown to locate mostly at clay layer edges. They become likely subject of interaction with various exposed layer sites and with existed Ti-pillar, as evident from SEM micrograph (d) imaging the effect of intercalated molecules on the etched clay structure. For the highest loaded sample (of 9.67 wt % FePc), the complex appears in micrograph (e) as ordered nanocrystallites (of 50 – 90 nm) extending to the edges of the overlying clay crystals, being different from original and modified bentonites. They exhibit some intercalation and interaction features, as documented in SEM micrograph (f) by deformed bentonite structure showing layered flowery shapes crowded with the complex species.

3.3. Surface Dispersion Characteristics of the Immobilized FePc Complex

In the present study, H_2-chemisorption at 300°C was applied for determining the degree of dispersion of immobilized FePc, applying some precautions as discussed elsewhere [28, 36]. For all immobilized FePc @ Ti-PILB samples, the obtained chemisorption isotherms showed almost monolayer coverage (Figure **7**). As the neat Ti-PILB support exhibited nearly undetectable H_2 –uptakes up to ~250 Torr, so the considerable uptakes on the immobilized FePc samples can be referred to highly dispersed nature of the complex. Dispersion parameters derived from the obtained chemisorption isotherms for immobilized FePc samples are given in Table **4**. They include the net adsorption uptakes after correction for the neat support (n_{H2}), metallic surface area (S_{FePc}), considering FePc as a plane quadratic molecule (D_{4h} symmetry) of 1.23 nm^2 area, [22] stoichiometry of H_2 adsorption (n_{H2}/n_{Fe}^{2+}) [24, 28, 36], assuming equal distribution of (100), (010) and

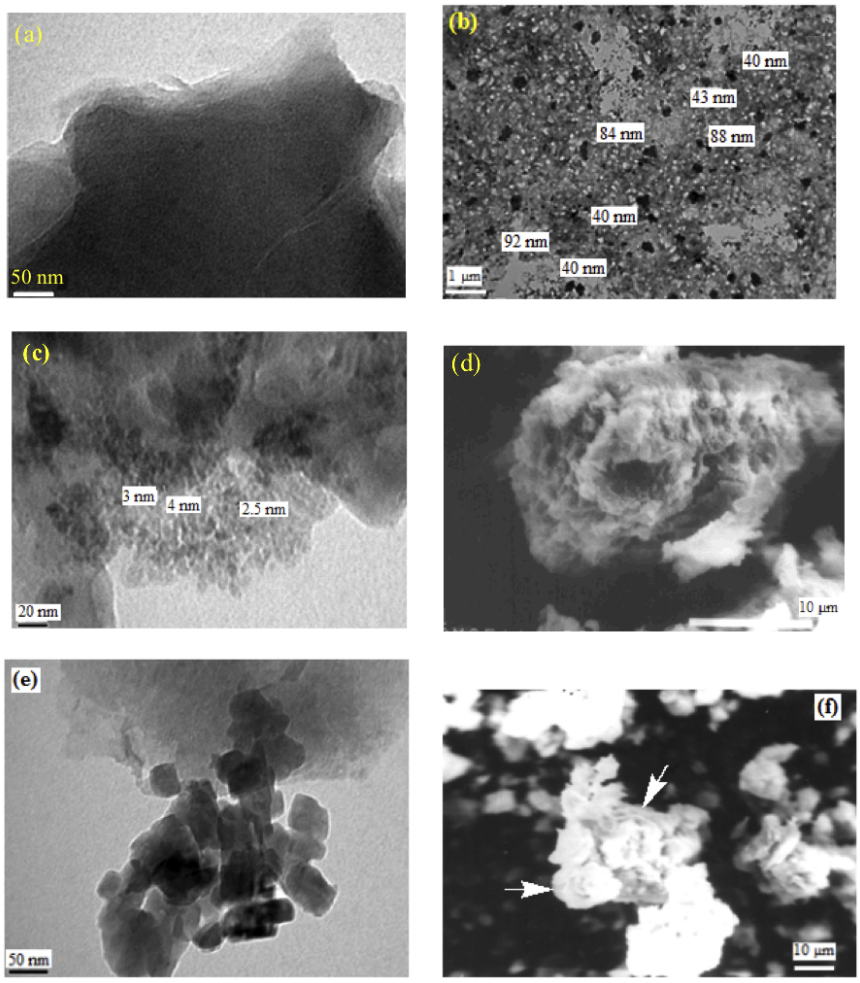

Figure 6: TEM of: (**a**) pure bentonite, (**b**) Ti-PILB, (**c**) 0.5 FePc@Ti-PILB, (**e**) 9.67 FePc@Ti-PILB and SEM of: (**d**) 0.5 FePc@Ti-PILB and (**f**) 9.67 FePc@TI-PILB.

(001) crystallite surfaces so that one Fe^{2+} is situated per 3.69 nm^2 area, and apparent degree of dispersion $[D]_{app}$ [36].

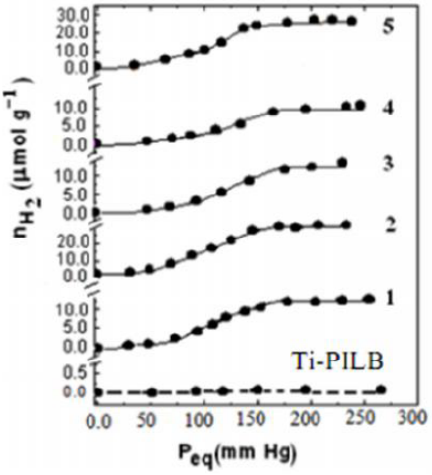

Figure 7: H_2-chemisorption isotherms at 300 °C on neat Ti-PILB support and various FePc@Ti-PILB samples of different FePc loadings (wt %): 1- 0.50, 2- 1.00, 3- 4.78, 4- 7.00 and 5- 9.67.

The results of Table **4** indicate that, the stoichiometry of H_2 adsorption (n_{H2} / n_{FePc}^{2+}) over diluted sample (of 0.5 wt % FePc) is close to 2:1. This may imply that FePc molecules, below the monolayer formation (α_{FePc}= 0.1), are accessible to H_2 from both sides, *i.e.*, through axial ligations to vacant d-orbitals of the central Fe^{2+} ion. Such facile accessibility is favored by an inclined edge-on interaction, between N's of FePc macrocyclic system and clay edge OH sites, via asymmetric BrÖnsted interaction [29, 36, 48]. It is characterized by higher degree of complex dispersion $[D]_{app}$ and increased metallic surface area (S_{FePc}).For higher loaded samples, of FePcwt % > 0.5 and ≤ 7.0, approaching monolayer formation (α_{FePc}= 1.0), H_2–adsorption stoichiometry becomes almost 1:1. FePc molecules seem to be accessible to H_2 from only one side, suggesting their deeper location in clay interlayers, parallel to silicate layer planes. This may allow the interaction between Fe^{2+} [with filled d_{π} (eg) orbitals] and Al^{3+} ions in octahedral sheets [22, 29] *i.e.*, via cation exchange/ substitution mechanism involving

Table 4: Dispersion Parameters of the Immobilized FePc in FePc@Ti-PILB Catalytic System Derived from H_2 Chemisorption and Specific Rate Constants (k_S) of ODH Reaction over Various Samples

Catalyst	n_{H2} (mmol g^{-1}_{FePc})	Stoich. (n_{H2}/n_{Fe}^{2+})	S_{FePc} ($m^2 g^{-1}_{FePc}$)	$[D]_{app}$	k_s (μmol g^{-1} s^{-1})
ATB					0.48
Ti- PILB					0.32
FePc@Ti-PILB of FePc wt %:					
0.50	1.84	1.97 (2:1)	44.3	0.522	2.21
1.00	1.23	0.91 (1:1)	59.1	0.317	1.83
4.78	0.17	1.31 (1:1)	8.2	0.096	2.05
7.00	0.13	0.70 (1:1)	6.3	0.070	1.41
9.67	0.32	0.52 (1:2)	30.8	0.091	1.88

octahedral coordination [22]. Interaction between N's of FePc and interlayer weaker acid sites cannot also be ruled out [36, 49]. By the influence of aggregated titania pillar, FePc molecules are enforced to stagger during intercalation into Ti-PILB galleries, (by *Domino effect*), and to lie in lower degrees of dispersion with smaller metallic surface areas (S_{FePc}). For the sample of 9.6 wt% FePc loading (exceeding monolayer formation), adsorption stoichiometry approaches 1:2, confirming the presence of the complex as clusters of probably dimeric units. In this instance, formation of some nanocrystallites with much less degree of dispersion may be displayed, where Fe-Fe interaction predominates (cf., TEM in Figure **6**).

3.4. Catalytic Performance of Immobilized FePc@Ti-PILB Samples in Oxidative Dehydrogenation (ODH) of Ethyl Benzene (EB)

In this part, the FePc@Ti-PILB nanocomposite system under investigation is applied as a tailored catalyst for oxidative dehydrogenation of ethyl benzene, capable of favoring hydrogen abstraction from hydrocarbons over the oxygen insertion in the olefins formed. In preliminary experiments, the reaction was carried out for 1 h over the 0.5 FePc@Ti-PILB sample, by adopting a dynamic air flow rate ranged between 5 and 40 ml min^{-1} and EB feed rate ranged between 0.5 and 6 ml h^{-1}, at temperatures varied between 300°C and 400°C. Higher temperatures were avoided for expected changes in complex structure, probable thermodynamic reversibility and enhanced rate of side reactions, *e.g.*, disproportionation and dealkylation [50]. Optimized conditions for the EB – ODH process were found as follows: EB feed rate = 2 ml min^{-1}, reaction temperature = 400°C,dynamic air flow rate = 15 ml min^{-1}, EB /air ratio = 0.223 % (V/V) and catalyst sample weight = 1g.

The activity parameters obtained at optimized oxidative conditions are depicted in Figure **8** (a), showing a significant increase in % conversion (X) by increasing % loading of FePc (only 9.3% being achieved in presence of neat Ti-PILB). Markedly high selectivity to styrene (S_{sty}), between 96 and 99 %, can be observed for all the immobilized samples (only 75.5 % with neat Ti-PILB). Specific reaction rate constants (k_s, mol s^{-1} g^{-1}) [14] included in Table **4** confirm the markedly higher activity values for immobilized complex samples, compared with neat Ti-PILB support. The pure polycrystalline FePc was completely inactive.

In Figure **8** (b), the turnover frequency, TOF, (h^{-1}) [43] is shown to decrease sharply by increasing % loading of FePc. The linear logarithmic relationship constructed in Figure **8** (c), between TOF and apparent degree of complex dispersion $[D]_{app}$, fitting an empirical equation of the type, log TOF = A + B log $[D]_{app}$ (where constants A = 1.4 mol sty / molFePc . h and B = 1.6 a.u.), highlights direct dependence of TOF on surface dispersion and mode of orientation of FePc complex. Figure **8** (b) demonstrates also synergistic combination of factors influencing selective production of styrene using the FePc @ Ti-PILB nanocomposite systems under study. They involve redox factor, linked with dispersion and mode of orientation of FePc complex, which are dependent on % loading and acid-base balance factor, represented by BrÖnsted acid site density (D_{SiO^-}), enhanced markedly through intercalation of FePc molecules and their interaction mainly with tetrahedral silica sites. For diluted samples, of higher FePc dispersion, the facile inclined edge-on

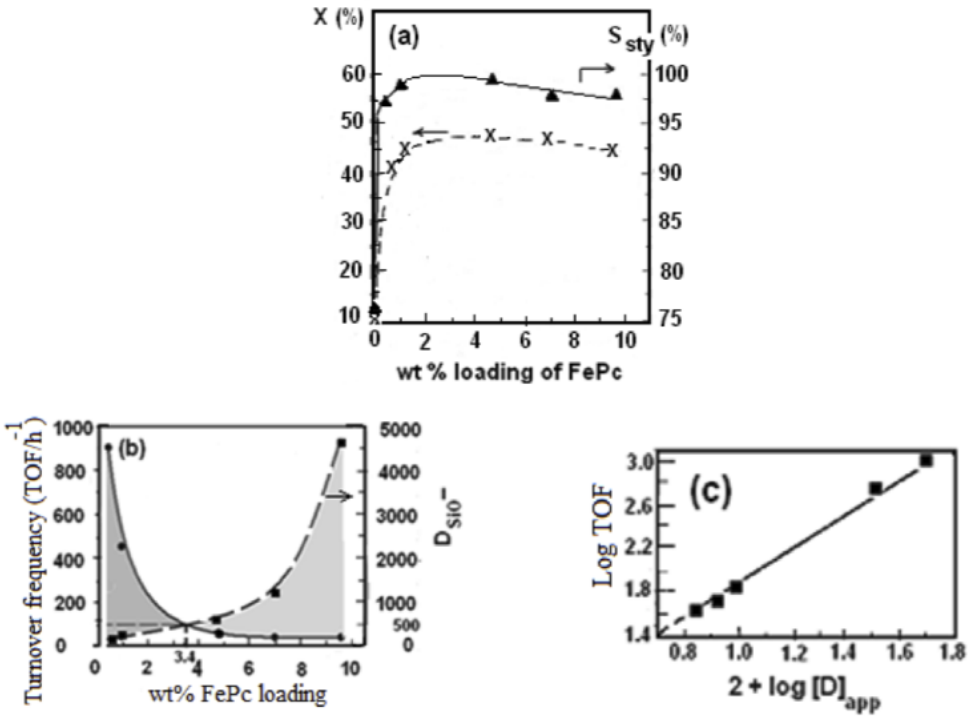

Figure 8: Catalytic activity parameters of FePc@Ti-PILB nanocomposite systems in ODH of EB as a function of FePc loading (wt %): (**a**) % conversion (X) and selectivity to styrene (S_{sty}) and (**b**) TOF in synergistic correlation with interlayer BrÖnsted acid site density (D_{SiO^-}) and % FePc loading (redox factor). (**c**): logarithmic correlation of TOF and apparent degree of surface dispersion $[D]_{app}$ of FePc.

orientation of complex molecules favours higher TOF values with reasonably high selectivity to styrene (S_{sty}). Here, FePc redox factor seems to predominate (Scheme **1**).

$$Fe^{2+}\ Pc + O_2 \rightarrow Fe^{3+}\ Pc + O_2^{-\cdot} \quad (1)$$

$$Fe^{3+}\ Pc + C_6H_5\text{-}C_2H_5 \rightarrow H^{\delta}\rightarrow Fe^{3+}Pc + C_6H_5 - CH_2CH_2^{+}$$

(Axially modified $Fe^{3+}Pc$)

↓

$$Fe^{2+}\ Pc + 2\ H^{+} + C_6H_5{-}CH{=}CH_2 \quad (2)$$

$$O_2^{-\cdot} + \text{Clay Brönsted acid sites (or 2 } H^{+}) \rightarrow HO_2^{\cdot} \quad (3)$$

$$HO_2^{\cdot} + C_6H_5{-}C_2H_5 \rightarrow C_6H_5 - CH_2CH_2^{\cdot} + H_2O_2 \rightarrow C_6H_5{-}CH{=}CH_2 \quad (4)$$

$$H_2O_2 \rightarrow H_2O + \tfrac{1}{2}\ O_2 \quad (5)$$

Scheme 1: Proposed reaction mechanism for ODH of EB, in O_2 flow environment, functioned Predominantly by FePc redox pair effect with some synergistic combination of clay BrÖnsted acid sites for production of styrene.

According to this scheme, under oxidative conditions, the initiation step involves formation of $O_2^{-\cdot}$ radicals, through interaction of Fe (II) Pc with dioxygen [51]. In the second redox step, abstraction of β-H atom from EB to produce styrene proceeds via formation of axially modified Fe (III) Pc($H^{\delta}\dashrightarrow Fe^{3+}$ Pc) [14, 24]. Styrene may also be produced by synergistic combination of clay BrÖnsted acid sites, as in the third and fourth steps. The dioxygen reappears with traces of water molecules in the last step. A parallel redox cycle involving pillar Ti^{4+}/Ti^{3+} pairs, based on Mars-van Krevelen redox mechanism [14, 52] may take place as in Scheme **2**.

For higher loaded samples, of lower FePc dispersion, associated with a marked increase in surface charge site densities (D_{SiO^-}), the TOF tends to decrease sharply but with much higher selectivity values (S_{sty}). Selective production of styrene can be mainly controlled by clay acid-base balance effect, as presented in Scheme **3**. The proposed mechanism [43, 50, 52] reveals adsorption of EB on an acid site, abstraction of β-H from EB by basic OH site adjacent to acid site, formation of an anion vacancy via desorption of water at t > 350°C, filling of the anionic vacancy by O^- species from adsorbed O_2 and abstraction of α-H

from EB by the O^- species, to produce styrene and basic OH group.

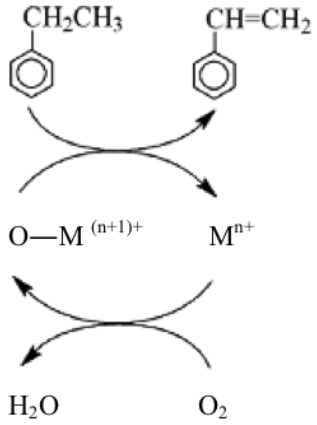

Scheme 2: Redox cycle of Ti-pillar species (Ti^{4+}/Ti^{3+} pairs), in the modified clay interlayers, as functioned in ODH of EB, in O_2 flow environment.

Moreover, as neat Ti-PILB support shows some conversion of EB with noticeable selectivity to styrene, one can accept that a certain controllable extent of acid-base pairs has to be available for the ODH reaction using the studied FePc @ Ti-PILB system. For instance, an optimized synergistic correlation is realized in Figure **8** (b), where an optimum TOF of about $120h^{-1}$ with maximum selectivity (99 %) to styrene can be achieved at 3.4 wt % FePc loading, exhibitingD_{SiO^-} of 500 sites nm^{-2}. The FePc redox pair effect seems to predominate below this loading, while clay acid-base pair balance effect becomes likely prevailing beyond it.

4. CONCLUSIONS

The hybrid catalytic system under study consisted of iron (II) phthalocyanine (FePc) immobilized, in different loadings between 0.5 and ~ 10 wt %, into acid treated bentonite modified by pillaring with titania nanoparticles (88 nm). The incorporated titania in clay interlayers exhibited weaker interaction with tetrahedral silica through occupation of some exchange sites. In diluted samples of < 1.0 wt % FePc, the complex seemed to collect at clay layer edges, in some edge-on oriented profile, restricted by located Ti-pillar. In higher loaded samples (≥ 1.0 wt % FePc), intercalated complex molecules, probably parallel to silicate layer planes, faced several interactions with Ti-pillar as well as with different interlayer sites. Through these interactions, several silanol and aluminol sites were exposed, density of which displayed considerable increase by increasing the FePc % loading. Applying this hybrid nanocatalytic system in ODH of EB under optimized oxidative conditions, both degree of EB conversion and selectivity to styrene showed a rapid increase with the increase in complex loading. The reaction TOF was directly dependent on the apparent

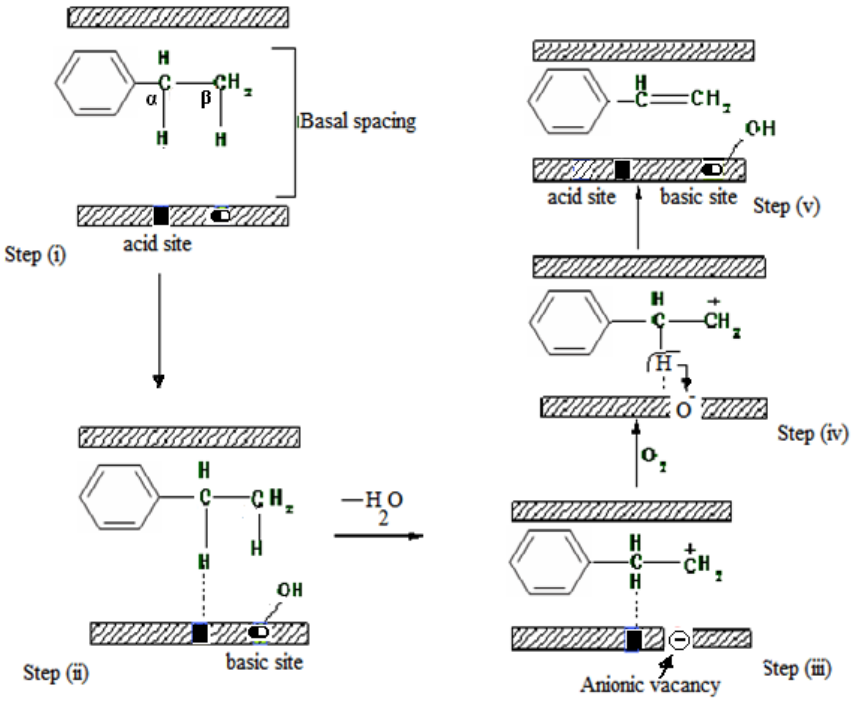

Scheme 3: Proposed reaction mechanism for ODH of EB to styrene functioned predominantly by acid – base pair effect in the modified clay galleries.

degree of complex dispersion. Synergistic combination of factors influencing selective production of styrene in presence of FePc @ Ti-PILB nanocomposite system showed that the optimum TOF of $120h^{-1}$ to selectively produce styrene (99 %) could be achieved at 3.4 wt % FePc loading. Below this loading, redox pair factor linked with dispersion and mode of orientation of FePc complex was predominating. Beyond it, acid-base pair balance effect, which is represented by BrÖnsted acid site density (D_{SiO^-}) enhanced by intercalated FePc molecules in clay interlayers, was prevailing.

REFERENCES

[1] Sarmiente RDC, Bello PJA. Appl Clay Sci 2001; 18: 173-81. http://dx.doi.org/10.1016/S0169-1317(00)00022-3

[2] M'bodj O, Arigui NK, Ayadi MT, Magnin A. J Colloid Interf Sci 2004; 273: 675-84.

[3] Bhattacharyya KG, Gupta SS. Chem Eng J 2008; 136: 1-13. http://dx.doi.org/10.1016/j.cej.2007.03.005

[4] Ikhsan J, Wells JD, Johnson BB, Angove MJ. Colloids Surf. A 2005; 252: 33-41. http://dx.doi.org/10.1016/j.colsurfa.2004.10.011

[5] Kim JO, Lee SM, Jeon C. Chem Eng Res Design 2014; 92: 368-74. http://dx.doi.org/10.1016/j.cherd.2013.07.020

[6] Nagy NM, Konya J. J Colloid Interf Sci 2006; 295: 173-80. http://dx.doi.org/10.1016/j.jcis.2005.07.065

[7] Bourg IC, Sposito G, Bourg ACM. J Colloid Interf Sci 2007; 312: 297-310. http://dx.doi.org/10.1016/j.jcis.2007.03.062

[8] Jozefaciuk G, Bowanko G. Clays Clay Miner 2002; 50: 771-83. http://dx.doi.org/10.1346/000986002762090308

[9] Bieseki L, Treichel H, Araujo AS, Pergher SBC. Appl Clay Sci 2013; 85: 46-52. http://dx.doi.org/10.1016/j.clay.2013.08.044

[10] Molina CB, Calvo L, Gilarranz MA, Casas JA, Rodriguez JJ.J Hazard Mater 2009; 172: 214-23. http://dx.doi.org/10.1016/j.jhazmat.2009.06.161

[11] Kooli F, Liu Y, Alshahateet SF, Siril P, Brown R. Catal Today 2008; 131: 244-9. http://dx.doi.org/10.1016/j.cattod.2007.10.053

[12] Mata G, Trujillano R, Vicente MA, Korili SA, Gil A, Belver C,*et al*. Micropor Mesopor Mater 2009; 124: 218-26. http://dx.doi.org/10.1016/j.micromeso.2009.05.018

[13] Chmielarz L, Piwowarska Z, Kuśtrowski P, Węgrzyn A, Gil B, Kowalczyk A. Appl Clay Sci 2011; 53: 164-73. http://dx.doi.org/10.1016/j.clay.2010.12.009

[14] [14]Belkhadem F, Clacens JM, Bengueddach A, Figueras F. Appl Catal A: General 2006; 298: 188-93. http://dx.doi.org/10.1016/j.apcata.2005.10.007

[15] Arfaoui J, Boudali LK, Ghorbel A. Catal Commun 2006; 7: 86-90. http://dx.doi.org/10.1016/j.catcom.2005.09.003

[16] [16]Binitha NN, Sugunan S. Micropor Mesopor Mater 2006; 93: 82-89. http://dx.doi.org/10.1016/j.micromeso.2006.02.005

[17] Kun R, Mogyorosi K, Dekany I. Appl Clay Sci 2006; 32: 99-110. http://dx.doi.org/10.1016/j.clay.2005.09.007

[18] Wu Y, Zhang Y, Cheng J, Li Z, Wang H, Sun Q, *et al.* Micropor Mesopor Mater 2012; 162: 51-9. http://dx.doi.org/10.1016/j.micromeso.2012.04.046

[19] Mimura N, Masahiro S.Catal Lett 1999; 58: 59-62. http://dx.doi.org/10.1023/A:1019049127309

[20] Ikenaga Na, Tsuruda T, Senma K, Yamaguchi T, Sakurai Y, Suzuki T.Ind Eng Chem Res 2000; 39: 1228-34. http://dx.doi.org/10.1021/ie990426q

[21] Moparthi A, Uppaluri R, Gill BS.Chem Eng Res Design 2010; 88: 1088-101. http://dx.doi.org/10.1016/j.cherd.2010.01.013

[22] Hassan SA, Zahran AA, Yehia FZA.Adsorpt. Sci. Technol. 2002; 20: 269-83. http://dx.doi.org/10.1260/026361702760254450

[23] Bedioui F.Coord Chem Rev 1995; 144: 39-68. http://dx.doi.org/10.1016/0010-8545(94)08000-H

[24] Hassan SA, Sadek SA, Faramawy SM, Mekewi MA. Stud Surf Sci Catal 1996; 100: 407-18. http://dx.doi.org/10.1016/S0167-2991(96)80040-1

[25] Chibwe M, Ukrainczyk L, Boyed SA, Pinnavaia TJ.J Mol Catal A: Chem 1996; 113: 249-56.

[26] Alvaro M, Carbonell E, Espla M, Garcia H. Appl Catal B: Environ 2005; 57: 37-42. http://dx.doi.org/10.1016/j.apcatb.2004.10.003

[27] Kameyama H, Fumitaka N, Hattori T, Kameyama H. J Mol Catal A: Chem 2006; 258: 172-77.

[28] Hassan SA, Yehia FZ, Hassan HA, Sadek SA, Darwish AS. J Mol Catal A: Chem 2010; 332: 93-106.

[29] Hassan SA, Yehia FZ, Hamed AA, Zahran AA, Solyman SM. J Porous Mater 2011; 18: 1-11. http://dx.doi.org/10.1007/s10934-009-9350-z

[30] Jagtap N, Ramaswamy V. Clays Clay Miner 2006; 54: 54-61. http://dx.doi.org/10.1346/CCMN.2006.0540107

[31] Biernacka IK, Silva AR,Carvalho AP, Pires J, Freire C. J Mol Catal A: Chem 2007; 248: 135 -43.

[32] Arfaoui J, Boudali LK, Ghorbel A, Delahay G. J Phys Chem Solids 2008; 69: 1121-24. http://dx.doi.org/10.1016/j.jpcs.2007.10.045

[33] Moser FH, Thomas AL, Eds. The Phthalocyanine Manufacture and Applications, second ed. CRC Press, USA 1983.

[34] Sadek EM, Mekewi MA, Yehia FZ, Solyman SM, Hassan SA. Macromol Chem Phys 2001; 202: 1505-12. http://dx.doi.org/10.1002/1521-3935(20010601)202:9<1505::AID-MACP1505>3.0.CO;2-Y

[35] Sing KSW, Everret DH, Haul RAW, Moscou L, Pierotti RA, Rouquerol J, et al. Pure Appl Chem 1985; 57: 603-619. http://dx.doi.org/10.1351/pac198557040603

[36] Hassan SA, Hassan HA, Hashem KM, Abdel Dayem HM. Appl Catal A: General 2006; 300: 14-23. http://dx.doi.org/10.1016/j.apcata.2005.10.036

[37] Gupta S.S, Bhattacharyya KG. J Colloid Interf Sci 2006; 295: 21-32.

[38] Kita H, Henmi N, Shimazu K, Hattori H, Tanabe J. J Chem Soc Farad Trans 1981; 77: 2451-63. http://dx.doi.org/10.1039/f19817702451

[39] Zarzycki P, Thomas F.J Colloid Interf Sci 2006; 302: 547-59. http://dx.doi.org/10.1016/j.jcis.2006.06.044

[40] Yang X, Sun Z, Wang D, Forsling W.J Colloid Interf Sci2007; 308: 395-404. http://dx.doi.org/10.1016/j.jcis.2006.12.023

[41] Rodrigues MGF.Ceramica 2003; 49: 146-50.

[42] Rozalén M, Brady PV, Huertas FJ.J Colloid Interf Sci 2009; 333: 474-84. http://dx.doi.org/10.1016/j.jcis.2009.01.059

[43] Bautista FM, Campelo JM, Luna D, Marinas JM, Quiros RA, Romero AA. Appl Catal B 2007; 70: 611-20. http://dx.doi.org/10.1016/j.apcatb.2005.10.039

[44] Eren E, Afsin B, Onal Y.J Hazard Mater 2009; 161: 677-85. http://dx.doi.org/10.1016/j.jhazmat.2008.04.020

[45] Chmielarz L, Kustrowski P, Zbroja M, Lasocha AR, Dudek B, Dziembaj R. Appl Catal B: Environ 2003; 45: 103-16. http://dx.doi.org/10.1016/S0926-3373(03)00121-8

[46] Agoudjil N, Benkacem T. Desalination 2007; 206: 531-37. http://dx.doi.org/10.1016/j.desal.2006.03.580

[47] Letaïef S, Casal B, Aranda P, Martin LMA, Ruiz HE. Appl Clay Sci 2003; 22: 263-77. http://dx.doi.org/10.1016/S0169-1317(03)00079-6

[48] Halma M, Castro ADF, Gueho CT, Prevot V, Foranco C, Wypych F, et al. J Catal 2008; 257: 233-43. http://dx.doi.org/10.1016/j.jcat.2008.04.026

[49] Ozoemena K, Nyokong T. J Electroanal Chem 2005; 579: 283-89.

[50] Mathew Th, Malwadkar S, Pai S, Sharanappa N, Sebastian CP, Satyanarayana CVV, *et al*.Catal Lett 2003; 91: 217-24. http://dx.doi.org/10.1023/B:CATL.0000007158.88722.5e

[51] Haber J, Pamin K, Poltowicz J. J Mol Catal A: Chem 2004; 224: 153-59.

[52] Friedrich HB, Mahomed AS. Appl Catal A: General 2008; 347: 11-22. http://dx.doi.org/10.1016/j.apcata.2008.05.019

Received on 29-08-2015 Accepted on 09-09-2015 Published on 30-09-2015

http://dx.doi.org/10.15379/2408-9834.2015.02.02.03